Electron Beam Injector for Longitudinal Beam Physics Experiments*

J. G. Wang, D. X. Wang and M. Reiser
Laboratory for Plasma Research and Department of Electrical Engineering
University of Maryland, College Park, Maryland 20742

Abstract

Design parameters of the electron beam injector for longitudinal beam physics experiments are discussed. The performance characteristics of its components and the injector system is presented.

I. INTRODUCTION

An electron beam injector has been constructed to study problems of longitudinal beam in the University of Maryland electron beam transport experiment. These include studies of longitudinal pulse compression and resistive-wall instability. The injector consists of a variable-perveance gridded electron gun followed by three matching lenses and one induction module. In the compression experiment, it produces a 50 ns, 40 mA, 2-5 keV electron pulse with a time-dependent velocity spread. This beam will be injected into a 5-m long periodic transport channel with 36 short solenoid lenses. The pulse is expected to be compressed by a factor of 3 or greater when reaching the end of the channel. In the resistive-wall instability experiment, the injector produces a 5 ns, 100 mA and 2.5 keV beam pulse. This beam will be guided into a resistive-wall channel of a few meters length for the instability study. This paper reports on the design features and the performance of the injector components and system.

II. DESIGN STUDY OF THE LONGITUDINAL COMPRESSION AND INSTABILITY

2.1, Beam compression due to drift bunching

The design of the compression experiment applies to a beam with parabolic density distribution, that satisfies the longitudinal envelope equation [1]

$$Z_m'' - \frac{3gZ_i I_i}{\beta^3\gamma^5 I_0}\frac{1}{Z_m^2} - \frac{\varepsilon_L^2}{\gamma^4}\frac{1}{Z_m^3} = 0 \quad , \tag{1}$$

where $2Z_m$ is the bunch length, g is a factor related to the beam radius, I_0 is the characteristic current of electrons, and ε_L is the normalized longitudinal emittance. Assuming a K-V distribution [2], one applies the transverse envelope equation

$$R'' + \kappa R - \frac{K}{R} - \frac{\varepsilon_T^2}{R^3} = 0 \quad , \tag{2}$$

where R is the transverse envelope, κ is the periodic focusing function of the lens, ε_T is the transverse emittance, and K is the generalized perveance. The two equations are coupled by the g factor and the product KZ_m which is a constant during the compression due to the conservation of the total number of electrons. Solving Eqs. (1) and (2) numerically yields the beam envelopes in both transverse and longitudinal directions. In our 5-m long channel, the solenoid lenses are spaced at intervals of s=13.6 cm. Fig. 1 shows these results for the initial parameters I_i=40 mA, T_i=50 ns, E_{head}=3.3 keV, E_{center}=5.0 keV. These are typical operational parameters expected for the new injector.

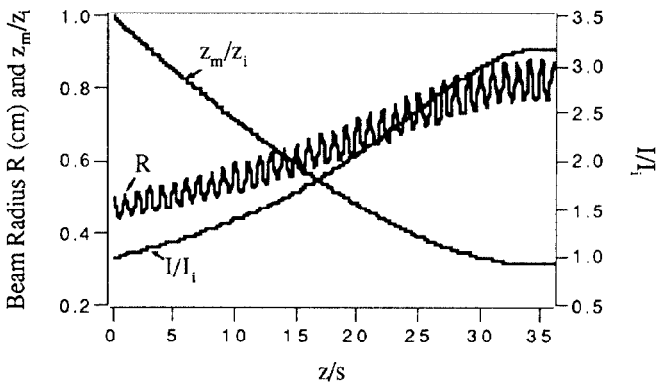

Fig. 1. Computer simulation of the longitudinal compression.

The experiment may have to compress a beam with an initial rectangular density distribution instead of a parabolic which is difficult to produce in practice. In this case the initial beam energy spread from head to tail will be smaller than the above results.

2.2, Resistive-wall instability

The resistive-wall instability growth rate is given by [3]

$$\omega_i \approx \frac{1}{2} v_0 R\left(\frac{4\pi\varepsilon_0\eta\lambda_0}{g}\right)^{1/2} , \tag{3}$$

where λ_0, v_0 are the unperturbed line charge density and drift velocity, respectively, η=q/m denotes the ratio of the charge and mass of the charged particles, and R is the resistance of the wall per unit length. This equation yields the number of e-folds per meter:

$$N = \left(\frac{1}{2}\eta\pi^2\varepsilon_0^2\right)^{1/4}\left(\frac{I}{g V^{1/2}}\right)^{1/2} R \quad . \tag{4}$$

For the instability experiment, an electron beam pulse has been designed with a pulse width of 5 ns, a beam energy of 2.5 keV, and a peak current of 100 mA. Assuming a resistance of 1 kΩ/m and g=2, Eq. (4) yields N≅0.1. A transport channel of a few meters in length would produce observable perturbation growth. These parameters will be scaled in the experiment. This is also the requirement for the electron beam injector in the instability study.

* Research Supported by U.S. Department of Energy.

0-7803-0135-8/91$01.00 ©IEEE

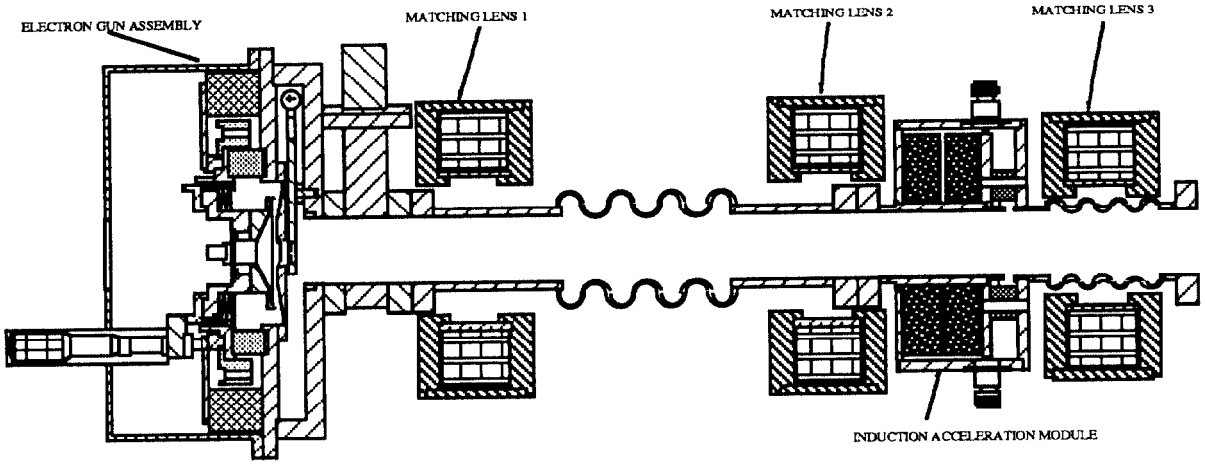

Fig. 2. Mechanical drawing of the electron beam injector system.

III. COMPONENTS OF ELECTRON BEAM INJECTOR

Fig. 2 shows the electron beam injector consisting of the following three major components:

3.1. Electron gun

The design of the variable-perveance gridded electron gun and its general performance characteristics were described in reference [4]. Since then, many improvements have been made to the gun, including replacement of the ML-EE55 oxide cathode by a Y646B dispenser cathode assembly. The A-K gap has been modified to vary from 0.93 cm to 2.3 cm, resulting in a perveance of 0.22 to 1.35 $\mu AV^{-3/2}$. This can be seen in Fig. 3, where the anode voltage is 2.5 kV.

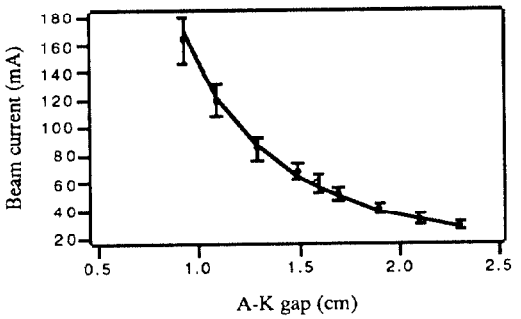

Fig. 3. Beam current vs. A-K gap where the smooth curve is from Child's law.

The beam emittance is measured by the pepper-pot method and calculated by [5]

$$\varepsilon_T = \frac{RD}{2z}\left(\frac{D_z}{D} - \frac{S_z}{S}\right)\left[1 - \left(\frac{S}{R}\right)^2\right]^{-1/2}, \qquad (5)$$

where R is the full beam radius, D and D_Z are the sizes of the pepper-pot hole and its image, S and S_Z are the radial distances from the axis of the centers of the pepper-pot hole and its image, respectively, z is the distance between the pepper-pot plate and the phosphor screen, The pepper-pot measurement yields a full beam emittance of 88 mm mrad with a standard deviation of 5 mm mrad.

3.2. Matching Lenses

There are three solenoid matching lenses in the injector system. The measured magnetic field $B_Z(r=0)$ is plotted in Fig. 4. The experimental data can be well fitted by the following function

$$B_z(0,\ z) = B_0\left(1 + \frac{z^2}{a^2}\right)^{-1} \exp\left(-\frac{z^2}{d^2}\right), \qquad (6)$$

where the two constants d and a are obtained from least-square fitting. The magnetic field components $B_z(r,z)$ and $B_r(r,z)$ off the z axis can then be calculated from Eq. (6) by power series expansion. These data will be used to simulate beam dynamics in the compression and instability experiments.

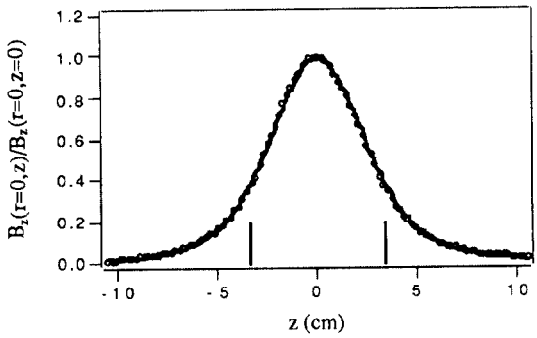

Fig. 4. The normalized magnetic field $B_Z(r=0)$ vs. z. The width of the lenses is indicated by the two parallel lines.

3.3. Induction acceleration module

The design and performance characteristics of the induction acceleration module can be found in reference [6]. The induction module consists of a single-turn primary around 2 ferrite cores with the beam completing the single-turn secondary. The gap voltage is controlled by a PFN circuit. The measured gap voltage is shown in Fig. 5, which is approximately t^2 shaped. This waveform can be changed to linear by modifying the PFN circuit.

The induction linac employs a pseudospark switch to control the PFN operation. This component provides superior

performance of the switch in the aspects of fast risetime, small jitter, current reversal capability, and long life time.

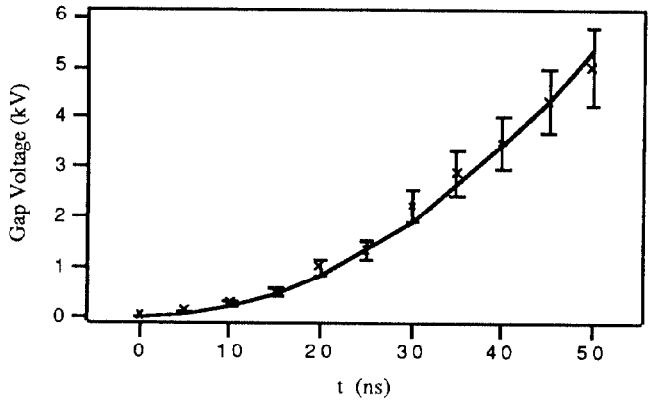

Fig. 5. Gap voltage vs. time in the induction module.

IV. BEAM CHARACTERISTICS IN THE INJECTOR

The beam transport in the injector and its interaction with the induction gap has been measured with a ML-EE55 cathode installed in the gun. Figure 6 shows the beam envelope obtained by a phosphor screen, where the two maximums are at the lens centers and the beam waist is focused at the induction gap. The beam image and profile is measured at 2 cm after the induction gap, and is shown in Fig. 7. The intensity of the beam after the induction gap as a function of the charging voltage V_0 of the induction module is shown in Fig. 8, indicating the energy transfer from the induction gap to the beam. This is a time integrated picture and needs to be calibrated. Besides the energy transfer, the induction gap also acts as a focusing lens. Fig. 8 also plots the FWHM of the beam profile as a function of the charging voltage of the induction module, showing the stronger focusing effect at the larger gap voltage. The average beam energy after the induction gap is proportional to the product of the intensity and square of FWHM, which is the straight line in the plot.

The test of the injector with the Y646B dispenser cathode assembly in the gun is underway. The results will be reported elsewhere in the near future.

V. SUMMARY

An electron beam injector has been designed for the longitudinal compression and resistive wall instability experiments at the University of Maryland. The injector has been constructed and preliminarily tested, showing satisfactory performance. The final test of the injector system is underway. The longitudinal physics experiments are expected in the near future and their results will be reported elsewhere.

VI. REFERENCES

[1] T. Shea, E. Boggasch, Y. Chen, and M. Reiser, "The University of Maryland electron pulse compression experiment", Proceedings of the IEEE Particle Accelerator Conference, Chicago Ill., March 20-23, 1989.

[2] I. M. Kapchinskij and V. V. Vladimirskij, "Limitations of proton beam current in a strong focusing linear accelerator associated with the beam space charge", Proc. of Int. Conf. on High Energy Accel. and Instr., pp. 274-288, CERN, Geneva, 1959.

[3] J. G. Wang, M. Reiser, W. M. Guo, and D. X. Wang, "Theoretical study of the longitudinal instability and proposed experiment", to be published in Particle Accelerators.

[4] J. G. Wang, E. Boggasch, P. Haldman, D. Kehne, M. Reiser, T. Shea, and D. X. Wang, "Performance characteristics of a variable-perveance gridded electron gun", IEEE Trans. ED, **37**(12), pp. 2622-2628, Dec. 1990.

[5] J. G. Wang, D. X. Wang, and M. Reiser, "Beam emmitance measurement by the pepper-pot method", to be published in NIM, (A).

[6] J. G. Wang, D. X. Wang, E. Boggasch, D. Kehne, M. Reiser, and T. Shea, "Design and performance characteristics of a compact induction acceleration module for longitudinal compression experiments", NIM, (A)**301**, pp19-26, 1991.

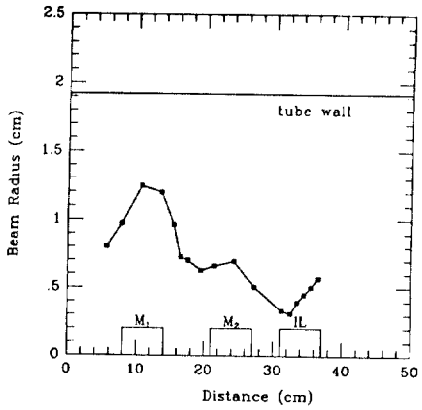

Fig. 6. Beam envelope in the injector system.

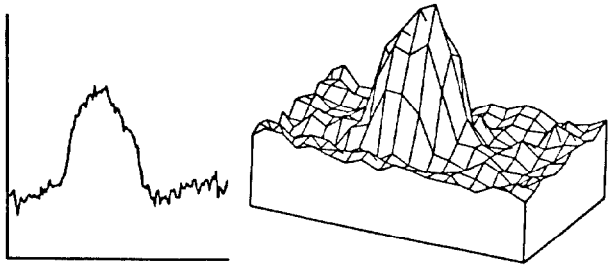

Fig. 7. Beam image and profile after the induction module.

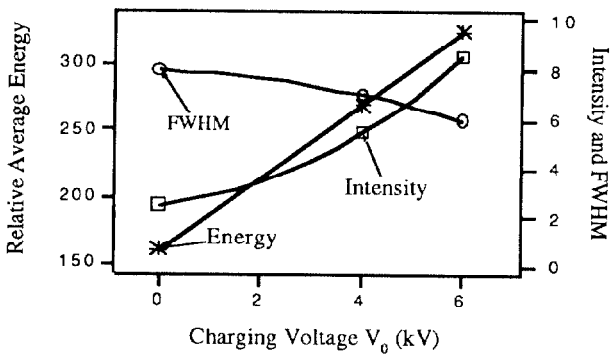

Fig. 8. Relative average beam energy after the induction gap vs. the charging voltage V_0 of the induction module.